Chapter 7

Numerical results: Orthotropic problems

7.1 Plane stress membrane cantilever under transverse tip loading

The plane stress membrane cantilever is depicted in Figure 7.1. $-u_{2_A}$ represents the reference displacement. Beam theory need not be exact.

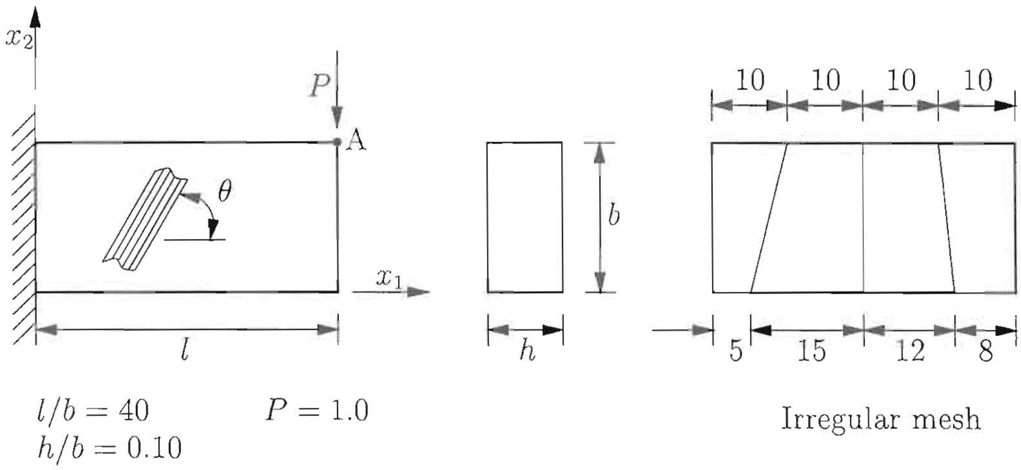

Figure 7.1: Cantilever under transverse tip loading and irregular mesh

7.1.1 Stacking sequence [0]

Table 7.1 reveals that for the regular mesh the 5β-NT element outperforms the other elements. For the irregular mesh the $8\beta*$-NT element is by far the most accurate. The 5β-NT element performs badly for this highly distorted mesh. For the irregular mesh the QC9D$*$ element also outperforms the 5β-NT element.

For this stacking sequence, Table 7.2 reveals that small values of γ predict more accurate displacements. For values of $\gamma > G_{12}$ the accuracy decreases drastically. The results with the choice of $\gamma = G_{12}$ are acceptable.

From the results presented in Table 7.3 it is clear that there is no significant influence of the integration schemes for the regular meshes. However, for the irregular mesh the $8\beta*$-NT element with full integration is the most accurate.

7.1.2 Stacking sequence [30]

As before, the 5β-NT element performs very well for the regular mesh, but for the irregular mesh the $8\beta*$-NT element is the most accurate (See Table 7.4). Note that the QC9D$*$ and the 5β-NT elements yield results an order of magnitude lower that the beam theory solution.

This stacking sequence is very sensitive to the value of γ (see Table 7.5). The best accuracy is obtained when γ is very small. With $\gamma = G_{12}$, the results are acceptable.

Table 7.6 reveals that for the regular meshes, the 5-point and 8-point integration schemes in combination with the locking correction outperform the other combinations without the locking correction. However, for the irregular mesh the $8\beta*$-NT element with full integration is again the most accurate.

7.1.3 Stacking sequence $[0/90]_s$

Numerical results for this stacking sequence are tabulated in Table 7.7. For the regular mesh all the elements are very accurate, except Q4. For the irregular mesh the $8\beta*$-NT element is the most accurate. Note that the 5β-NT element again yield results an order of magnitude lower that the beam theory solution. QC9D$*$ yields accurate results for this problem.

7.1.4 Stacking sequence $[30/-30]_s$

For this staking sequence the 5β-NT, $8\beta*$-NT and $9\beta*$-NT all yields very accurate results (See Table 7.8). For the irregular mesh the $8\beta*$-NT element is again the most accurate with the 5β-NT formulation an order of magnitude lower than the theoretical solution.

7.1.5 Stacking sequence $[0/45/-45/90]_s$

For the coarse meshes Table 7.9 reveals that the QC9D$*$ element is the most accurate, and for the refined meshes the 5β-NT element is the most accurate. For the irregular mesh the $8\beta*$-NT element is again the most accurate with the 5β-NT formulation an order of magnitude lower than the theoretical solution.

7.2 Clamped cylinder under internal pressure

Depicted in Figure 7.2, this problem was proposed by Haas and Lee [60]. u_{1_A} at $l/2$ is the reference displacement of interest.

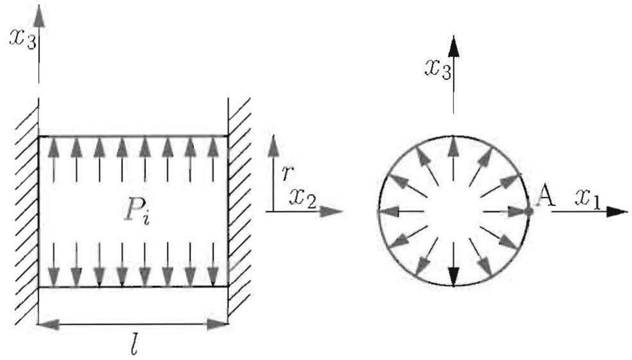

$E_{11} = 7.5 \times 10^6$
$E_{22} = 2.0 \times 10^6$
$G_{12} = 1.25 \times 10^6$
$G_{13} = G_{23} = 0.625 \times 10^6$
$\nu_{12} = 0.25$
$P_i = 6.4/\pi$
$r = 20$
$l = 20$

Figure 7.2: Clamped cylinder under internal pressure

7.2.1 Stacking sequence [90]

Numerical results for this stacking sequence are tabulated in Table 7.10. For $r/t = 20$ all the elements yields accurate results, with the $8\beta*$-NT/SA results slightly superior. For $r/t = 100$ the Q4/SA element yields highly accurate results. $8\beta*$-NT/SA compares very well with Q4/SA for all the meshes.

7.2.2 Stacking sequence $[-45/45]_s$

Numerical results for this stacking sequence are tabulated in Table 7.11. For $r/t = 20$ the $8\beta*$-NT/SA element yields the most accurate results. For $r/t = 100$ the $8\beta*$-NT/SA element with the 4×4 mesh is virtually converged. All the other elements yields comparable results for the 8×8 mesh.

7.2.3 Stacking sequence $[90/0]_s$

Numerical results for this stacking sequence are tabulated in Table 7.12. For $r/t = 20$ the Q4/SA element is the most accurate. All the elements converge from above. For $r/t = 100$ all the elements, except $8\beta*$-NT/SA, converge from above. The $8\beta*$-NT/SA element results are virtually converged for the coarse 4×4 mesh.

7.2.4 Stacking sequence $[0/90]_s$

Numerical results for this stacking sequence are tabulated in Table 7.13. Haas and Lee [60] did not perform this stacking sequence. For $r/t = 20$ all the elements converges monotonically from above. For $r/t = 100$ all the elements, except Q4/SA, oscillate around approximately 0.0008450. Q4/SA converge monotonically from above.

7.2.5 Stacking sequence [0]

Numerical results for stacking sequence are tabulated in Table 7.14. Again, Haas and Lee [60] did not perform this test. For $r/t = 20$ all the elements converge monotonically from above. For $r/t = 100$ QC9D∗/SA and 8β∗-NT/SA converge monotonically from above. Q4/SA and 9β∗-NT/SA oscillate around approximately 0.0005364.

7.3 Clamped hemisphere with 30^o hole

This problem was suggested by Moser and Schmid [61], and is depicted in Figure 7.3, showing the graded mesh proposed by Moser and Schmid. In this study, the benefit of the graded mesh is not exploited. Instead, the meshes are constructed using bisection.

7.3.1 Ply orientation $E_\theta = E_{11}$

Numerical results for this ply orientation are tabulated in Table 7.18. For the coarse mesh the 8β∗-NT/SA element is the most accurate at points A and C. At point B the Q4/SA element is the most accurate. Note that the Q4/SA element is the most accurate for the refined mesh at points A and C.

Table 7.16 reveals that for small values of γ the displacement at points A and B are the most accurate, while the best results are obtained at point C when γ is large.

Results in Table 7.17 shows that at point A the 8β∗-NT/SA element with the 8-point integration scheme is the most accurate for the coarse mesh. The performance of the elements with the locking correction is improved with the use of reduced integration. At points B and C the 8β-NT/SA element with the 8-point integration scheme is the most accurate for the coarse mesh. In general, the 8β-NT/SA element with the 8-point integration scheme is the most accurate.

7.3.2 Ply orientation $E_\phi = E_{11}$

Numerical results for this ply orientation are tabulated in Table 7.18. For the coarse mesh the Q4/SA element yields the most accurate results. For the refined meshes 8β∗-NT/SA is the most accurate at point C.

This ply orientation is insensitive to the value of γ. However, note that for both large and small values of γ the best displacement at point C is obtained (see Table 7.19).

Results in Table 7.20 shows that the 8β-NT/SA with the 8-point integration scheme gives the most accurate results in points A, B and C.

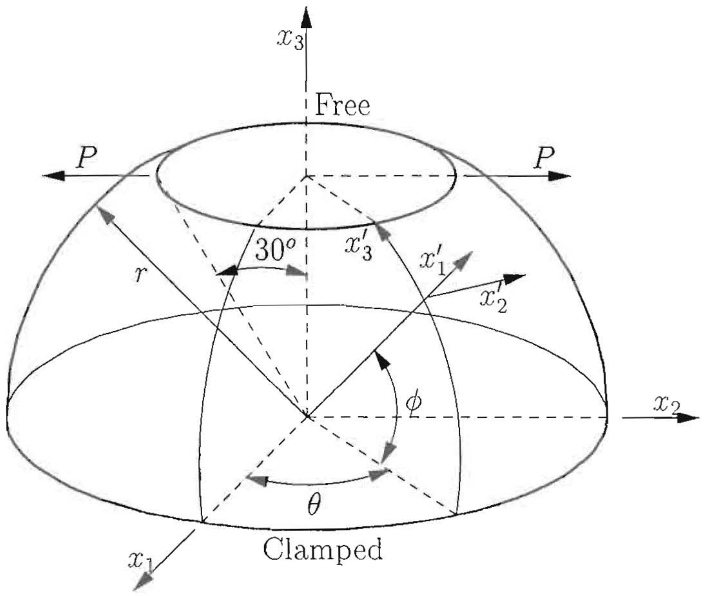

$E_{11} = 7.5 \times 10^6$ $\quad P = 2.0$ $\quad$ Case 1 : $E_\theta = E_{x_2'} = E_{11}$

$E_{22} = 2.0 \times 10^6$ $\quad t = 1.0$ $\quad$ Case 2 : $E_\phi = E_{x_3'} = E_{11}$

$G_{12} = 1.25 \times 10^6$ $\quad r = 100.0$

$\nu_{12} = 0.25$

$\nu_{23} = 0.45$

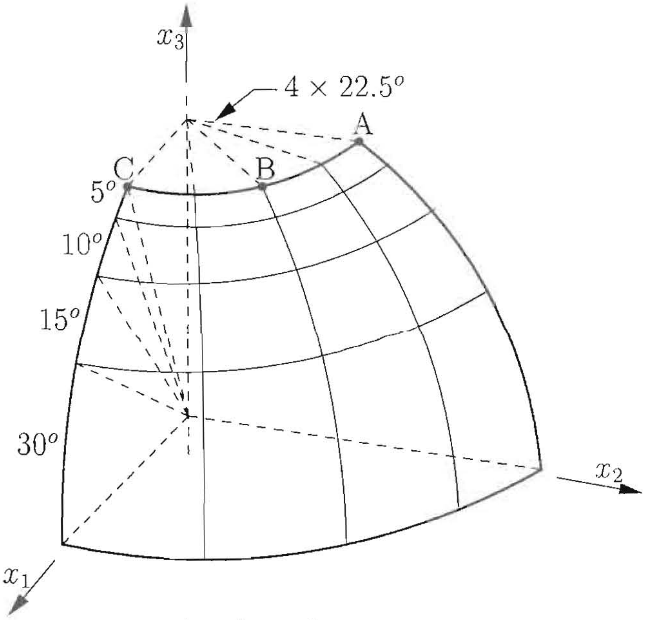

4×4 mesh

Figure 7.3: Clamped hemisphere with 30^o hole

7.4 Pre-twisted beam

The pre-twisted beam depicted in Figure 5.9 is used to illustrate the capability of the elements for warped geometries. For this new problems there are no known exact solutions. ($E_{11} = 30\times10^6, E_{22} = 0.75\times10^6, \nu_{12} = 0.28, G_{12} = 0.45\times10^6, G_{13} = 0.45\times10^6$ and $G_{23} = 0.375\times10^6$)

7.4.1 Stacking sequence $[0/90]_s$

Numerical results for this stacking sequence are tabulated in Table 7.21. All the elements converge monotonically from below for the in-plane shear loading condition ($\approx$ 0.3545). For the out-of-plane shear loading condition all the elements converge monotonically from above. All the elements yield approximately converged results for the coarse 1×6 mesh ($\approx$ 0.009544).

7.4.2 Stacking sequence $[-45/45]_s$

Numerical results for this stacking sequence are tabulated in Table 7.22. All the elements converge monotonically from below. In addition, the results predicted by the elements are very similar ($\approx$ 0.08723 for u_{3_A} and $\approx$ 0.03006 for u_{2_A}).

7.4.3 Stacking sequence $[30/60]_s$

Numerical results for this stacking sequence are tabulated in Table 7.23. All the elements converge monotonically from below to roughly 0.08939 for the in-plane shear and to roughly 0.02878 for the out-of plane shear.

Element	1×4	2×8	4×16	8×32	Irregular Mesh
Q4	0.03447	0.06269	0.07893	0.08440	0.01545
QC9D*	0.08485	0.08607	0.08632	0.08637	0.07768
5β-NT	0.08489	0.08588	0.08626	0.08636	0.03069
8β*-NT	0.08489	0.08620	0.08637	0.08638	0.08217
9β*-NT	0.08488	0.08612	0.08635	0.08638	0.08184
Beam theory			0.08533		

Table 7.1: Plane stress membrane cantilever (Stacking sequence [0]): Tip displacement $-u_{2_A}$

γ	Irregular mesh
$G_{12} \times 10^{-3}$	0.02992
$G_{12} \times 10^{-2}$	0.02990
$G_{12} \times 10^{-2}$	0.02972
$G_{12} \times 10^{0}$	0.02855
$G_{12} \times 10^{1}$	0.02549
$G_{12} \times 10^{2}$	0.02019
$G_{12} \times 10^{3}$	0.01750
Beam theory	0.08533

Table 7.2: Plane stress membrane cantilever (Stacking sequence [0]): Influence of γ on irregular mesh

Element	1×4	2×8	4×16	Irregular mesh
5 point integration				
$8\beta*$-NT	0.08489	0.08620	0.08637	0.07810
8β-NT	0.08488	0.08588	0.08626	0.02692
8 point integration				
$8\beta*$-NT	0.08489	0.08620	0.08637	0.07968
8β-NT	0.08488	0.08588	0.08626	0.02707
Full integration				
$8\beta*$-NT	0.08489	0.08620	0.08637	0.08217
8β-NT	0.08488	0.08588	0.08626	0.02855
Beam theory		0.08533		

Table 7.3: Plane stress membrane cantilever (Stacking sequence [0]): Effect of integration scheme order

Element	1×4	2×8	4×16	8×32	Irregular Mesh
Q4	0.004815	0.01734	0.06465	0.2221	0.002128
QC9D$*$	0.6114	0.9179	1.160	1.250	0.2938
5β-NT	1.300	1.296	1.293	1.295	0.1133
$8\beta*$-NT	1.230	1.130	1.220	1.270	1.250
$9\beta*$-NT	1.137	1.080	1.210	1.267	1.194
Beam theory			1.320		

Table 7.4: Plane stress membrane cantilever (Stacking sequence [30]): Tip displacement $-u_{2_A}$

γ	Irregular mesh
$G_{12} \times 10^{-3}$	0.09082
$G_{12} \times 10^{-2}$	0.08417
$G_{12} \times 10^{-2}$	0.07596
$G_{12} \times 10^{0}$	0.05908
$G_{12} \times 10^{1}$	0.03975
$G_{12} \times 10^{2}$	0.03509
$G_{12} \times 10^{3}$	0.03456
Beam theory	1.320

Table 7.5: Plane stress membrane cantilever (Stacking sequence [30]): Influence of γ on irregular mesh

Element	1×4	2×8	4×16	Irregular mesh
5 point integration				
$8\beta*$-NT	1.230	1.130	1.220	1.137
8β-NT	1.299	1.262	1.259	0.06053
8 point integration				
$8\beta*$-NT	1.230	1.130	1.220	1.182
8β-NT	1.299	1.262	1.259	0.06076
Full integration				
$8\beta*$-NT	1.230	1.130	1.220	1.250
8β-NT	1.290	1.254	1.257	0.05908
Beam theory			1.320	

Table 7.6: Plane stress membrane cantilever (Stacking sequence [30]): Effect of integration scheme order

Element	1×4	2×8	4×16	8×32	Irregular Mesh
Q4	0.04261	0.09658	0.1414	0.1600	0.01660
QC9D*	0.1645	0.1665	0.1671	0.1673	0.1407
5β-NT	0.1646	0.1665	0.1671	0.1673	0.04056
$8\beta*$-NT	0.1646	0.1668	0.1672	0.1673	0.1576
$9\beta*$-NT	0.1646	0.1665	0.1672	0.1673	0.1556
Beam theory			0.1663		

Table 7.7: Plane stress membrane cantilever (Stacking sequence $[0/90]_s$): Tip displacement $-u_{2_A}$

Element	1×4	2×8	4×16	8×32	Irregular Mesh
Q4	0.004276	0.01651	0.05879	0.1654	0.001777
QC9D$*$	0.3126	0.3707	0.3998	0.4136	0.1021
5β-NT	0.4226	0.4034	0.4143	0.4208	0.03139
$8\beta*$-NT	0.4081	0.4181	0.4151	0.4184	0.3831
$9\beta*$-NT	0.4081	0.4067	0.4128	0.4180	0.3752
Beam theory			0.4292		

Table 7.8: Plane stress membrane cantilever (Stacking sequence $[30/-30]_s$): Tip displacement $-u_{2_A}$

Element	1×4	2×8	4×16	8×32	Irregular Mesh
Q4	0.006177	0.02293	0.07128	0.1510	0.002386
QC9D$*$	0.2329	0.2380	0.2399	0.2405	0.1052
5β-NT	0.2373	0.2382	0.2397	0.2404	0.02269
$8\beta*$-NT	0.2373	0.2400	0.2406	0.2408	0.2229
$9\beta*$-NT	0.2373	0.2392	0.2403	0.2407	0.2141
Beam theory			0.2351		

Table 7.9: Plane stress membrane cantilever (Stacking sequence $[0/45/-45/90]_s$): Tip displacement $-u_{2_A}$

Element	4×4	8×8	16×16
$r/t = 20.0$			
Q4/SA	0.0003596	0.0003699	0.0003727
QC9D$*$/SA	0.0003641	0.0003736	0.0003738
$8\beta*$-NT/SA	0.0003764	0.0003744	0.0003739
$9\beta*$-NT/SA	0.0003643	0.0003737	0.0003738
Haas and Lee		0.0003781	
$r/t = 100.0$			
Q4/SA	0.002040	0.002055	0.002051
QC9D$*$/SA	0.002225	0.002077	0.002052
$8\beta*$-NT/SA	0.002081	0.002055	0.002050
$9\beta*$-NT/SA	0.002225	0.002076	0.002052
Haas and Lee		0.002044	

Table 7.10: Clamped cylinder under internal pressure (Stacking sequence [90]): Radial displacement u_{1_A}

Element	4×4	8×8
$r/t = 20.0$		
Q4/SA	0.0002250	0.0002307
QC9D$*$/SA	0.0002352	0.0002334
$8\beta*$-NT/SA	0.0002369	0.0002335
$9\beta*$-NT/SA	0.0002355	0.0002335
Haas and Lee	0.0002402	
$r/t = 100.0$		
Q4/SA	0.001088	0.001068
QC9D$*$/SA	0.001137	0.001063
$8\beta*$-NT/SA	0.001063	0.001061
$9\beta*$-NT/SA	0.001129	0.001062
Haas and Lee	0.001068	

Table 7.11: Clamped cylinder under internal pressure (Stacking sequence $[-45/45]_s$): Radial displacement u_{1_A}

Element	4×4	8×8	16×16
$r/t = 20.0$			
Q4/SA	0.0001797	0.0001788	0.0001786
QC9D$*$/SA	0.0001797	0.0001791	0.0001787
$8\beta*$-NT/SA	0.0001811	0.0001792	0.0001787
$9\beta*$-NT/SA	0.0001797	0.0001791	0.0001787
Haas and Lee		0.0001783	
$r/t = 100.0$			
Q4/SA	0.0008455	0.0008447	0.0008441
QC9D$*$/SA	0.0008904	0.0008450	0.0008439
$8\beta*$-NT/SA	0.0008435	0.0008439	0.0008439
$9\beta*$-NT/SA	0.0008900	0.0008450	0.0008439
Haas and Lee		0.0008422	

Table 7.12: Clamped cylinder under internal pressure (Stacking sequence $[90/0]_s$): Radial displacement u_{1_A}

Element	4×4	8×8	16×16
$r/t = 20.0$			
Q4/SA	0.0001841	0.0001822	0.0001818
QC9D$*$/SA	0.0001856	0.0001825	0.0001819
$8\beta*$-NT/SA	0.0001854	0.0001825	0.0001818
$9\beta*$-NT/SA	0.0001856	0.0001825	0.0001819
$r/t = 100.0$			
Q4/SA	0.0008630	0.0008462	0.0008453
QC9D$*$/SA	0.0008817	0.0008444	0.0008452
$8\beta*$-NT/SA	0.0008442	0.0008459	0.0008453
$9\beta*$-NT/SA	0.0008812	0.0008444	0.0008452

Table 7.13: Clamped cylinder under internal pressure (Stacking sequence $[0/90]_s$): Radial displacement u_{1_A}

Element	4×4	8×8	16×16
$r/t = 20.0$			
Q4/SA	0.0001141	0.0001123	0.0001119
QC9D$*$/SA	0.0001147	0.0001123	0.0001119
$8\beta*$-NT/SA	0.0001139	0.0001122	0.0001119
$9\beta*$-NT/SA	0.0001146	0.0001123	0.0001119
$r/t = 100.0$			
Q4/SA	0.0005340	0.0005370	0.0005364
QC9D$*$/SA	0.0005630	0.0005371	0.0005364
$8\beta*$-NT/SA	0.0005417	0.0005371	0.0005364
$9\beta*$-NT/SA	0.0005340	0.0005370	0.0005364

Table 7.14: Clamped cylinder under internal pressure (Stacking sequence $[0]$): Radial displacement u_{1_A}

Element	4×4	8×8	16×16
Radial displacement at A			
Q4/SA	0.7099E-04	1.034E-04	1.151E-04
QC9D$*$/SA	0.7151E-04	1.035E-04	1.141E-04
$8\beta*$-NT/SA	0.7268E-04	1.036E-04	1.142E-04
$9\beta*$-NT/SA	0.7170E-04	1.035E-04	1.141E-04
Moser and Schmid		$\approx 1.15E-04$	
Radial displacement at B			
Q4/SA	-0.3804E-04	-0.4316E-04	-0.4463E-04
QC9D$*$/SA	-0.3535E-04	-0.4285E-04	-0.4428E-04
$8\beta*$-NT/SA	-0.3563E-04	-0.4287E-04	-0.4429E-04
$9\beta*$-NT/SA	-0.3543E-04	-0.4286E-04	-0.4428E-04
Moser and Schmid		$\approx -0.44E-04$	
Radial displacement at C			
Q4/SA	0.04328E-04	0.1242E-04	0.1208E-04
QC9D$*$/SA	0.08398E-04	0.1283E-04	0.1213E-04
$8\beta*$-NT/SA	0.08456E-04	0.1280E-04	0.1212E-04
$9\beta*$-NT/SA	0.08442E-04	0.1283E-04	0.1212E-04
Moser and Schmid		$\approx 0.12E-04$	

Table 7.15: Clamped hemisphere with 30^o hole (Ply orientation $E_\theta = E_{11}$): Radial displacement

Element	4×4
Radial displacement at A	
$G_{12} \times 10^{-3}$	0.6929E-04
$G_{12} \times 10^{-2}$	0.6928E-04
$G_{12} \times 10^{-2}$	0.6917E-04
$G_{12} \times 10^{0}$	0.6879E-04
$G_{12} \times 10^{1}$	0.6843E-04
$G_{12} \times 10^{2}$	0.6836E-04
$G_{12} \times 10^{3}$	0.6834E-04
Moser and Schmid	$\approx 1.15E-04$
Radial displacement at B	
$G_{12} \times 10^{-3}$	-0.3580E-04
$G_{12} \times 10^{-2}$	-0.3580E-04
$G_{12} \times 10^{-2}$	-0.3577E-04
$G_{12} \times 10^{0}$	-0.3567E-04
$G_{12} \times 10^{1}$	-0.3561E-04
$G_{12} \times 10^{2}$	-0.3561E-04
$G_{12} \times 10^{3}$	-0.3561E-04
Moser and Schmid	$\approx -0.44E-04$
Radial displacement at C	
$G_{12} \times 10^{-3}$	0.1033E-04
$G_{12} \times 10^{-2}$	0.1033E-04
$G_{12} \times 10^{-2}$	0.1037E-04
$G_{12} \times 10^{0}$	0.1052E-04
$G_{12} \times 10^{1}$	0.1073E-04
$G_{12} \times 10^{2}$	0.1079E-04
$G_{12} \times 10^{3}$	0.1080E-04
Moser and Schmid	$\approx 0.12E-04$

Table 7.16: Clamped hemisphere with 30^o hole (Ply orientation $E_\theta = E_{11}$): Influence of γ on 4×4 mesh

Element	4×4	8×8
Radial displacement at A		
5 point integration		
$8\beta*$-NT/SA	0.7470E-04	1.039E-04
8β-NT/SA	0.7150E-04	1.032E-04
8 point integration		
$8\beta*$-NT/SA	0.7472E-04	1.039E-04
8β-NT/SA	0.7152E-04	1.032E-04
Full integration		
$8\beta*$-NT/SA	0.7268E-04	1.036E-04
8β-NT/SA	0.6879E-04	1.029E-04
Moser and Schmid	$\approx 1.15E-04$	
Radial displacement at B		
5 point integration		
$8\beta*$-NT/SA	-0.3691E-04	-0.4301E-04
8β-NT/SA	-0.3765E-04	-0.4384E-04
8 point integration		
$8\beta*$-NT/SA	-0.3693E-04	-0.4301E-04
8β-NT/SA	-0.3766E-04	-0.4284E-04
Full integration		
$8\beta*$-NT/SA	-0.3563E-04	-0.4287E-04
8β-NT/SA	-0.3567E-04	-0.4268E-04
Moser and Schmid	$\approx -0.44E-04$	
Radial displacement at C		
5 point integration		
$8\beta*$-NT/SA	0.09401E-04	0.1290E-04
8β-NT/SA	0.1203E-04	0.1266E-04
8 point integration		
$8\beta*$-NT/SA	0.09410E-04	0.1289E-04
8β-NT/SA	0.1203E-04	0.1266E-04
Full integration		
$8\beta*$-NT/SA	0.08456E-04	0.1280E-04
8β-NT/SA	0.1052E-04	0.1260E-04
Moser and Schmid	$\approx 0.12E-04$	

Table 7.17: Clamped hemisphere with 30^o hole (Ply orientation $E_\theta = E_{11}$): Effect of integration scheme order

Element	4×4	8×8	16×16
Radial displacement at A			
Q4/SA	1.102E-04	1.600E-04	1.766E-04
QC9D$*$/SA	0.9654E-04	1.617E-04	1.769E-04
$8\beta*$-NT/SA	1.041E-04	1.627E-04	1.769E-04
$9\beta*$-NT/SA	0.9743E-04	1.617E-04	1.769E-04
Moser and Schmid		$\approx 1.8E-04$	
Radial displacement at B			
Q4/SA	-0.6605E-04	-0.6850E-04	-0.7056E-04
QC9D$*$/SA	-0.5242E-04	-0.6950E-04	-0.7074E-04
$8\beta*$-NT/SA	-0.5705E-04	-0.7004E-04	-0.7078E-04
$9\beta*$-NT/SA	-0.5301E-04	-0.6953E-04	-0.7075E-04
Moser and Schmid		$\approx -0.7E-04$	
Radial displacement at C			
Q4/SA	0.3680E-04	0.3952E-04	0.3792E-04
QC9D$*$/SA	0.2594E-04	0.3791E-04	0.3833E-04
$8\beta*$-NT/SA	0.2972E-04	0.3996E-04	0.3836E-04
$9\beta*$-NT/SA	0.2636E-04	0.3954E-04	0.3833E-04
Moser and Schmid		$\approx 0.4E-04$	

Table 7.18: Clamped hemisphere with 30^o hole: (Ply orientation $E_\phi = E_{11}$): Radial displacement

Element	4×4
Radial displacement at A	
$G_{12} \times 10^{-3}$	1.094E-04
$G_{12} \times 10^{-2}$	1.094E-04
$G_{12} \times 10^{-2}$	1.093E-04
$G_{12} \times 10^{0}$	1.090E-04
$G_{12} \times 10^{1}$	1.088E-04
$G_{12} \times 10^{2}$	1.088E-04
$G_{12} \times 10^{3}$	1.088E-04
Moser and Schmid	$\approx 1.8E-04$
Radial displacement at B	
$G_{12} \times 10^{-3}$	-0.6335E-04
$G_{12} \times 10^{-2}$	-0.6333E-04
$G_{12} \times 10^{-2}$	-0.6329E-04
$G_{12} \times 10^{0}$	-0.6315E-04
$G_{12} \times 10^{1}$	-0.6307E-04
$G_{12} \times 10^{2}$	-0.6306E-04
$G_{12} \times 10^{3}$	-0.6305E-04
Moser and Schmid	$\approx -0.7E-04$
Radial displacement at C	
$G_{12} \times 10^{-3}$	0.3641E-04
$G_{12} \times 10^{-2}$	0.3641E-04
$G_{12} \times 10^{-2}$	0.3639E-04
$G_{12} \times 10^{0}$	0.3637E-04
$G_{12} \times 10^{1}$	0.3642E-04
$G_{12} \times 10^{2}$	0.3643E-04
$G_{12} \times 10^{3}$	0.3643E-04
Moser and Schmid	$\approx 0.4E-04$

Table 7.19: Clamped hemisphere with 30^o hole (Ply orientation $E_\phi = E_{11}$): Influence of γ on 4×4 mesh

Element	4×4	8×8
Radial displacement at A		
5 point integration		
$8\beta*$-NT/SA	1.067E-04	1.631E-04
8β-NT/SA	1.144E-04	1.632E-04
8 point integration		
$8\beta*$-NT/SA	1.068E-04	1.631E-04
8β-NT/SA	1.144E-04	1.632E-04
Full integration		
$8\beta*$-NT/SA	1.041E-04	1.627E-04
8β-NT/SA	1.090E-04	1.626E-04
Moser and Schmid	$\approx 1.8E-04$	
Radial displacement at B		
5 point integration		
$8\beta*$-NT/SA	-0.5882E-04	-0.7026E-04
8β-NT/SA	-0.6696E-04	-0.6999E-04
8 point integration		
$8\beta*$-NT/SA	-0.5884E-04	-0.7026E-04
8β-NT/SA	-0.6699E-04	-0.6999E-04
Full integration		
$8\beta*$-NT/SA	-0.5705E-04	-0.7004E-04
8β-NT/SA	-0.6315E-04	-0.6973E-04
Moser and Schmid	$\approx -0.7E-04$	
Radial displacement at C		
5 point integration		
$8\beta*$-NT/SA	0.3113E-04	0.4009E-04
8β-NT/SA	0.3922E-04	0.3981E-04
8 point integration		
$8\beta*$-NT/SA	0.3114E-04	0.4009E-04
8β-NT/SA	0.3924E-04	0.3981E-04
Full integration		
$8\beta*$-NT/SA	0.2972E-04	0.3996E-04
8β-NT/SA	0.3637E-04	0.3974E-04
Moser and Schmid	$\approx 0.4E-04$	

Table 7.20: Clamped hemisphere with 30^o hole (Ply orientation $E_\phi = E_{11}$): Effect of integration scheme order

Element	1×6	2×12	4×24	8×48
In-plane shear: u_{3_A}				
QC9D*/SA	0.03525	0.03533	0.03535	0.03535
8β*-NT/SA	0.03532	0.03542	0.03544	0.03545
9β*-NT/SA	0.03532	0.03541	0.03544	0.03545
Out-of-plane shear: u_{2_A}				
QC9D*/SA	0.009570	0.009548	0.009520	0.009518
8β*-NT/SA	0.009594	0.009574	0.009547	0.009544
9β*-NT/SA	0.009594	0.009573	0.009546	0.009544

Table 7.21: Pre-twisted beam (Stacking sequence $[0/90]_s$): Numerical results

Element	1×6	2×12	4×24	8×48
In-plane shear: u_{3_A}				
QC9D*/SA	0.06968	0.07973	0.08489	0.08721
8β*-NT/SA	0.07000	0.07990	0.08495	0.08723
9β*-NT/SA	0.06998	0.07990	0.08495	0.08723
Out-of-plane shear: u_{2_A}				
QC9D*/SA	0.02445	0.02763	0.02928	0.02997
8β*-NT/SA	0.02542	0.02838	0.02956	0.03006
9β*-NT/SA	0.02542	0.02836	0.02955	0.03006

Table 7.22: Pre-twisted beam (Stacking sequence $[-45/45]_s$): Numerical results

Element	1×6	2×12	4×24	8×48
In-plane shear: u_{3_A}				
QC9D*/SA	0.08230	0.08779	0.08899	0.08938
8β*-NT/SA	0.08552	0.08815	0.08903	0.08939
9β*-NT/SA	0.08487	0.08809	0.08902	0.08939
Out-of-plane shear: u_{2_A}				
QC9D*/SA	0.02669	0.02834	0.02867	0.02877
8β*-NT/SA	0.02823	0.02857	0.02872	0.02878
9β*-NT/SA	0.02794	0.02855	0.02872	0.02878

Table 7.23: Pre-twisted beam (Stacking sequence $[30/60]_s$): Numerical results